JOURNAL OF MATERIALS SCIENCE 31 (1996) 875–880

Microstructure and fracture toughness of nickel particle toughened alumina matrix composites

XUDONG SUN*, J. A. YEOMANS
Department of Materials Science and Engineering, University of Surrey, Guildford, Surrey, GU2 5XH, UK

Al_2O_3–Ni composite materials have been made by a hot pressing technique. Two composite microstructures, i.e. a dispersive distribution of nickel particles and a network distribution of nickel particles in an alumina matrix, have been produced. The fracture toughness of the composite materials has been measured by a double cantilever beam method. Both composites are tougher than the virgin alumina matrix. The fracture toughness of the composite with a network microstructure is much higher and has a more desirable *R*-curve behaviour than the composite with a microstructure of dispersed particles. For the particulate dispersion microstructure, the main limitation to toughening is the lack of plastic deformation of the ductile nickel due to the pull out of nickel particles, indicating weak bonding at the Al_2O_3/Ni interface. For the network microstructure composite, the gauge length of the ductile phase is much larger, allowing the ductile nickel to stretch to failure between the crack faces. A large extent of nickel plastic deformation has been observed, and the weak bonding at the Al_2O_3/Ni interface can promote partial debonding and contribute further to toughening.

1. Introduction

Monolithic ceramics possess the attractive properties of high hardness, chemical stability, refractory character and low density. However, they are brittle at low temperatures because of a fundamental lack of dislocation mobility and insufficient slip systems. The toughness of ceramics can be improved by the incorporation of various reinforcements [1], among which ductile reinforcement toughening is one of the most promising toughening mechanisms, as demonstrated in several metal phase toughened ceramic matrix composites [2–11]. The toughness increment is mainly derived from the mechanism of crack bridging [12, 13] in which the ductile phase is stretched to failure between the crack surfaces, and the energy dissipation due to the plastic deformation of the ductile phase is the major contribution to the toughness of the composites. The increase in toughness, ΔG, can be estimated by [1]

$$\Delta G = \chi f \sigma_y R \tag{1}$$

where f is the area fraction of ductile phase intercepted by the crack, R is the radius of the ductile phase, σ_y is the yield stress of the ductile phase, and χ is a "work-of-rupture" parameter and is given by

$$\chi = \int_0^{u^*/R} \frac{\sigma(u)}{\sigma_y} d\frac{u}{R} \tag{2}$$

in which u is the crack opening displacement and u^* is the crack opening displacement upon rupture of the ductile ligament. The efficient use of the inherent toughness of the ductile phase in the composite needs a proper control of several factors. These include the physical and chemical compatibility of the ceramic and the ductile phase, mechanical properties of the ductile phase, microstructure of the composite, and the ceramic–ductile phase interfacial properties.

This work investigates the effect of microstructural factors and interfacial bonding on the toughening of Al_2O_3–20 vol % Ni composites. Two composite microstructures, i.e. a dispersive distribution of nickel particles and a network distribution of nickel particles in an alumina matrix, have been produced. The relationship between microstructure and resistance curve (*R*-curve) behaviour of the composites has been studied.

2. Experimental procedure

2.1. Fabrication of the composites

The materials used for making the Al_2O_3–Ni composite materials were AKP-30 α-alumina powder and nickel powder. The alumina powder was supplied by Sumitomo Chemical Co. Ltd, Tokyo, Japan. According to the manufacturer's data, the purity of the alumina powder is 99.99% and the particle size is in the range 0.3–0.5 μm. The nickel powder was supplied by Goodfellow Advanced Materials, Cambridge, UK.

* *Present address*: Department of Materials Science and Engineering, Northeastern University, Shenyang Liaoning 110006, People's Republic of China

0022–2461

The purity of the nickel powder is 99.8% and particle size is in the range 2–7 μm.

Two powder blends, which differ in their distribution of nickel particles, were prepared. For both powder blends the proportions of alumina and nickel were calculated to give 20 vol % nickel in the final product by taking the theoretical densities as 8.902 $Mg\,m^{-3}$ for nickel [14] and 3.990 $Mg\,m^{-3}$ for alumina [15]. The theoretical density of the composite is calculated to be 4.96 $Mg\,m^{-3}$, assuming no reaction product is formed. Powder blend one was prepared by dry milling 500 g in total of alumina powder and nickel powder for 3 h in a polypropylene bottle. Alumina cylindrical milling media, with a total mass of half that of the powder blend, were added to promote mixing. It was anticipated that this method would produce an even distribution of discrete nickel particles throughout the composite.

The preparation of powder blend two was aimed at producing an interconnecting or network distribution of nickel particles in the powder blend. Alumina powder was mixed with water until the alumina particles agglomerated. The alumina was heated to 400 °C in air, held for 4 h then furnace cooled. The alumina bulk was then broken and ground into alumina aggregates. Alumina aggregates ranging from 150 to 356 μm in diameter were selected by sieving. Powder blend two, about 250 g in total, was prepared by dry milling the selected alumina aggregates with nickel powder for 3 h in a polypropylene bottle. Alumina cylindrical milling media with a total mass of a quarter of that of the powder blend were added to promote mixing. Since the alumina aggregates are much larger than the alumina particles of the alumina powder, the total surface area of unit weight alumina aggregates is much smaller than that of unit weight alumina particles. Thus, it was anticipated that the distribution of nickel particles in powder blend two would tend to be more like a network and less even than in powder blend one.

The powder blends were consolidated into composite specimens by hot pressing. About 25 g batches of powder blend were hot pressed in a 25 mm diameter graphite die heated by a graphite resistance heating element, both of which were protected from oxidation by an argon atmosphere. The hot pressing temperature was 1400 °C. All samples were heated at 20 °C min^{-1}. On reaching the hot pressing temperature, a uniaxial pressure of 30 MPa was applied. Both pressure and temperature were held for 30 min. The pressure was then released and the system allowed to cool to room temperature.

2.2. Characterization of composites

Specimens for microstructural characterization and subsequent indentation testing were cut on a small bench-top cutting-off machine (Struers, Accutom) using a diamond cut-off wheel. The specimens were polished to a 1 μm diamond surface finish using a semi-automatic polishing machine (Struers, Planopol-2/Pedemax-2). Phase identification was performed on samples cut from the centre of hot pressed bodies using X-ray diffractometry (XRD) on a Philips PW1050 X-ray diffractrometer.

Microstructural observations of polished surfaces and fracture surfaces of the composite were performed using a Stereoscan 250 (Leica, Cambridge) scanning electron microscope (SEM). Transmission electron microscopy (TEM) specimens were made by cutting a thin plate of about 300–400 μm in thickness from the bulk specimen, drilling discs 3 mm in diameter from the plate using a high speed drilling machine (Testbourne, Servo Products Co.), polishing the discs to a thickness of 100–200 μm, dimpling on a VCR D500 dimpler to a thickness of about 30–70 μm and then ion beam thinning to perforation using a Gatan ion-beam thinner. A Jeol 2000FX TEM operating at 200 kV was used to examine the specimens.

The final density of the composite was determined by Archimedes' principle. The hot pressed samples were lightly abraded, to remove the skin which was likely to be of a different composition to the bulk of the samples, and then coated with wax prior to density measurement.

Hardness testing was performed on a Vickers pyramid diamond hardness testing machine (Vickers–Armstrongs Ltd). The specimens were polished to a 1 μm diamond surface finish before the tests. The load used was 20 kg, with a loading time of 5 s. Results were averaged over at least ten indentations per specimen.

The fracture toughness of the composites was evaluated using a modified double cantilever beam (DCB) method. The testing arrangement, specimen dimensions and equation for the fracture toughness calculation are described elsewhere [16]. The specimens were tested in the chamber of a Cambridge Instruments Stereoscan S 100, allowing *in situ* observation of crack growth.

3. Results and discussion

3.1. Microstructure of the composites

An SEM photomicrograph of the microstructure typical of the hot pressed specimens, made from powder blend one (specimen H1), is shown in Fig. 1. It can be seen that nickel particles are evenly distributed throughout the matrix. Phase identification by X-ray diffraction techniques showed that the composite was composed of alumina and nickel. Fig. 2 shows the typical microstructure of the alumina matrix in the hot pressed specimens. The average grain size is about 0.45 μm, i.e. within the 0.3–0.5 μm range of the raw alumina powder, indicating that alumina grains did not grow substantially during the hot pressing process. It can be seen that the alumina matrix is quite dense. Occasionally, porosity and defects can be observed in alumina grains. The defects can be dislocations, subgrain boundaries and, occasionally, stacking faults (Fig. 3). Fig. 4 is a transmission electron photomicrograph of a typical Al_2O_3/Ni interface. There is no evidence of $NiAl_2O_4$ spinel phase at the interface. Small irregularities exist at the Al_2O_3/Ni interface. This may be caused by the dissolution of a small

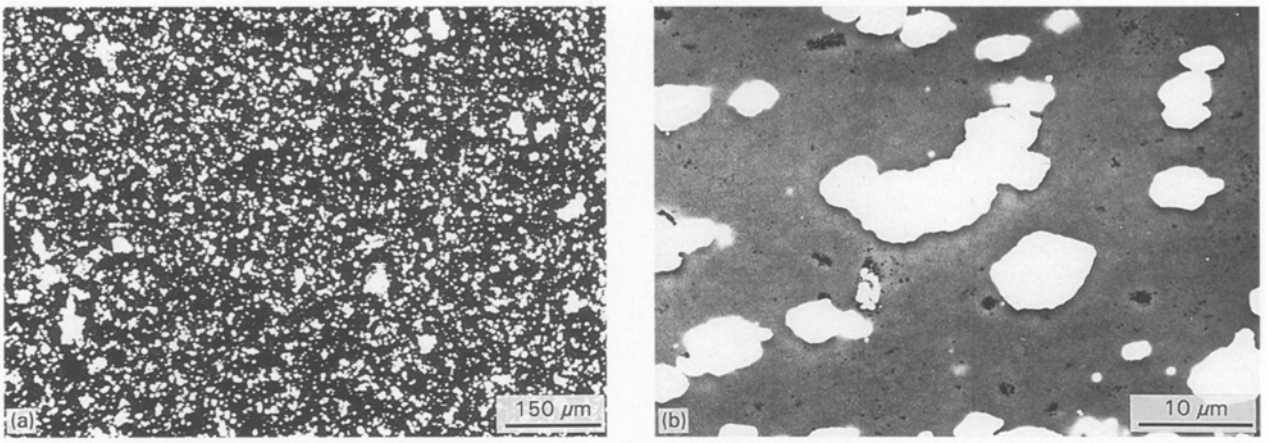

Figure 1 (a) Low and (b) high-magnification SEM photomicrographs showing the microstructure of specimen H1.

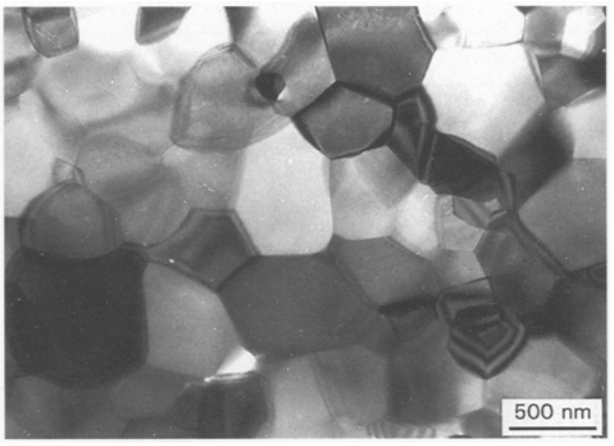

Figure 2 Microstructure of the alumina matrix in the composites (TEM).

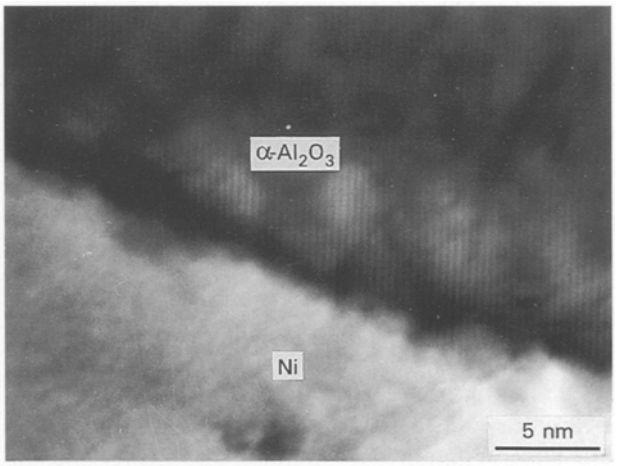

Figure 4 Al_2O_3/Ni interface in the composites (TEM).

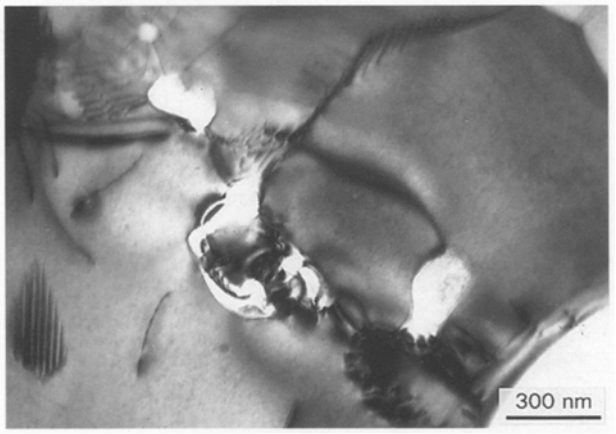

Figure 3 Defects in the alumina matrix of the composites (TEM).

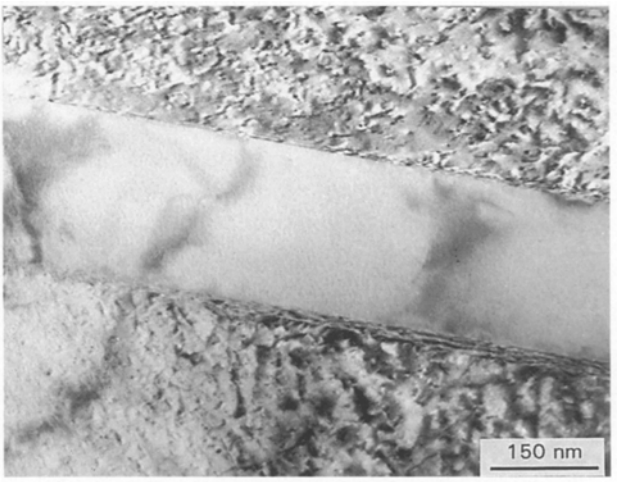

Figure 5 Existence of dense dislocations and twin boundaries in the nickel particles of the composites.

amount of alumina in nickel. Such dissolution has been identified in other works [17–20]. A high density of dislocations and some twin boundaries exist in the nickel phase (Fig. 5). Selected area diffraction patterns show that the twins are {1 1 1} twins. These defects are most likely to be due to the mismatch in the coefficients of thermal expansion of nickel and alumina, causing the nickel to experience stresses during cooling from the processing temperature.

The microstructure of the specimen made from powder blend two (specimen H2) is shown in Fig. 6. Nickel is distributed along the boundaries of the alumina aggregates and most of the grains are in contact with one another, making a network-like microstructure. Thus, the nickel phase is more continuous than that in specimen H1. The alumina agglomerates are elongated in a direction perpendicular to the hot pressing direction. The Al_2O_3/Ni interface under TEM observation is similar to that in specimen H1.

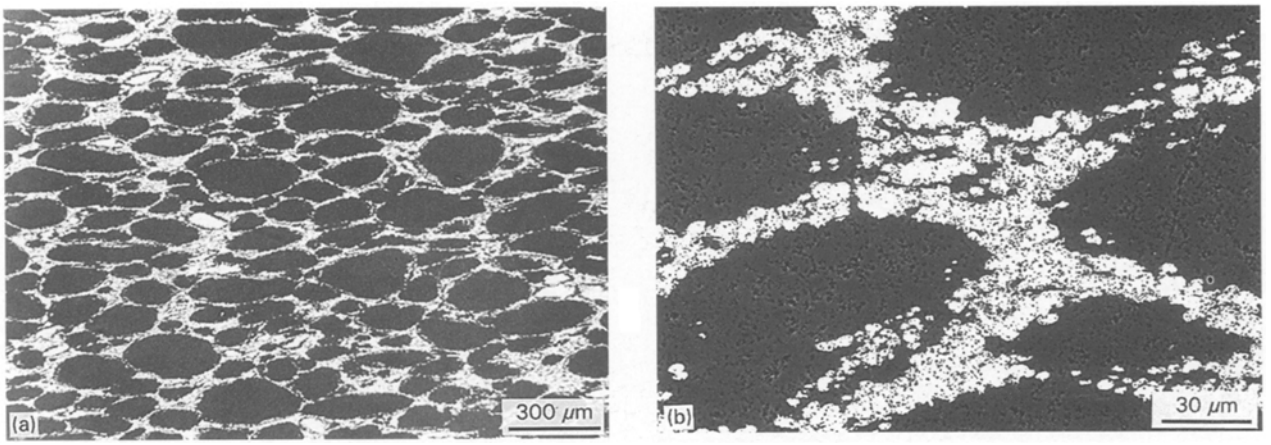

Figure 6 (a) Low and (b) high magnification SEM photomicrographs showing the microstructure of specimen H2.

TABLE I Observations and properties of the composites

Specimen	Observations	Density (% theoretical)	Hardness (GPa)	K_{Ic} (MPa $m^{1/2}$)
Al_2O_3	Al_2O_3	99.0	23.3	3.1
H1	Al_2O_3 + Ni particles	99.6	11.4	5.6
H2	Al_2O_3 + Ni network	99.2	10.6	13.1

3.2. Density, hardness and fracture toughness of the composites

Densities, mean values of hardness and fracture toughness of the specimens are given in Table I. It can be seen that it is possible to produce composite materials which contain only alumina and nickel and are very close to theoretical density. The hardness values of all the composite specimens are lower than the values for pure alumina.

Results of the DCB testing of specimens H1 and H2 are shown in Fig. 7. Resistance-curve behaviour is observed for both composites. The fracture toughness of the matrix alumina is 3.1 MPa $m^{1/2}$. The toughness values of both composites (specimens H1 and H2) are higher than that of the parent matrix. The fracture toughness increment over alumina achieved by specimen H1 is comparatively small (ΔK_{IC} = 2.5 MPa $m^{1/2}$). Specimen H2 is much tougher (ΔK_{IC} = 10.0 MPa $m^{1/2}$) than both the alumina matrix and specimen H1.

3.3. Interaction of cracks with nickel particles

To gain the maximum benefit from the nickel phase it must participate in crack bridging. Bridging of cracks by the nickel phase can be observed sometimes in specimen H1. However, in many cases cracks go along the Al_2O_3/Ni interface (Fig. 8). This is due to the weak bonding between nickel and alumina. Fig. 9 shows the fracture surface of specimen H1 after DCB testing. A lot of holes exist on the fracture surface, indicating pull out of the nickel particles and weak bonding between the nickel and the alumina matrix. This restricts seriously the plastic deformation of the nickel particles during the fracture of the composite, and is the main limitation for toughening. Sometimes, nickel

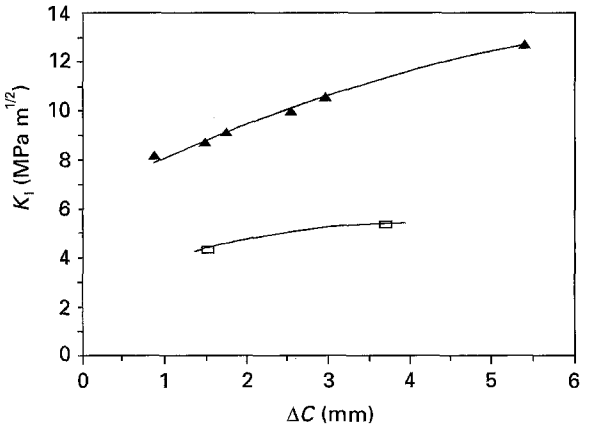

Figure 7 Stress intensity factor, K_I, against increase in crack length, ΔC, obtained by the DCB testing method for specimens H1 (□) and H2 (▲).

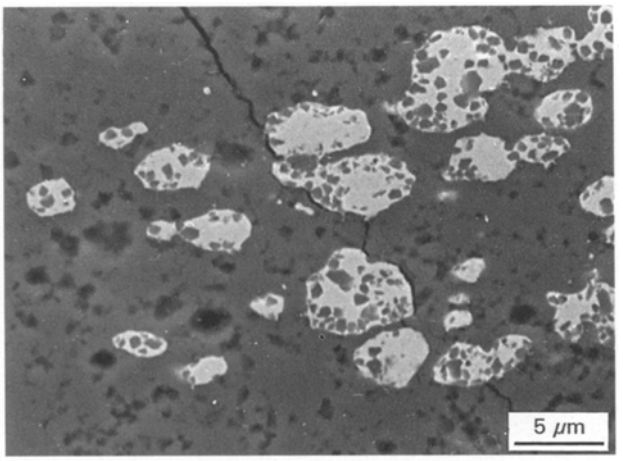

Figure 8 SEM photomicrograph showing a crack going along the Al_2O_3/Ni interface in specimen H1.

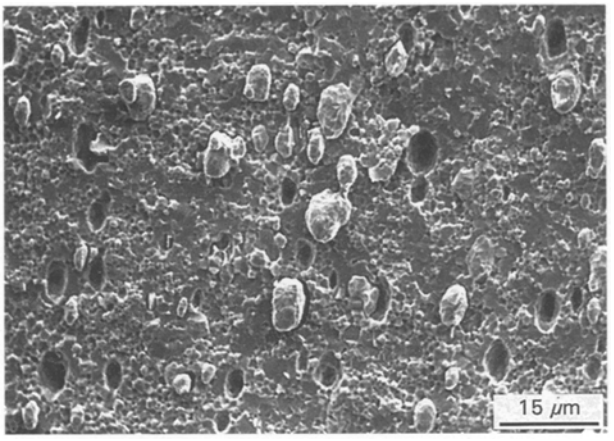

Figure 9 Fracture surface of specimen H1, showing the holes left by the pull out of the nickel particles (SEM).

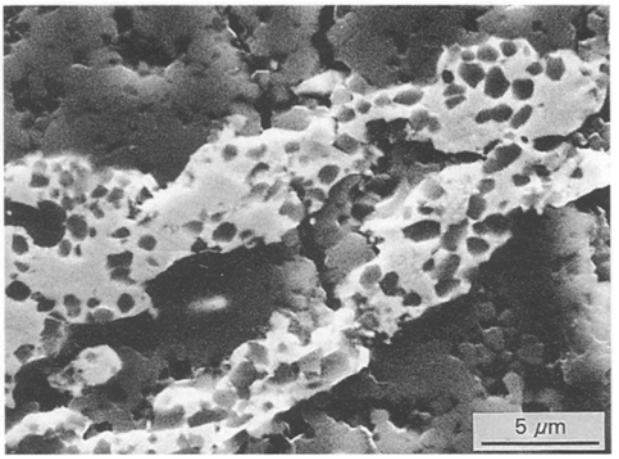

Figure 11 Bridging of a crack by the nickel phase in specimen H2 (SEM).

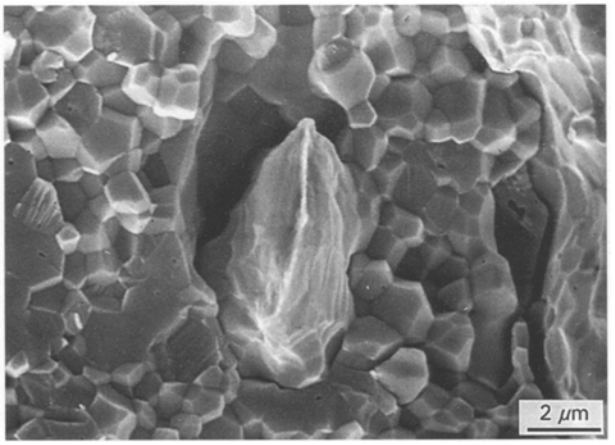

Figure 10 A nickel particle which has failed by necking to a line in specimen H1 (SEM).

particles that have been stretched to failure can be observed (Fig. 10), and these particles contribute more to toughening. However, the fractured nickel particles on the fracture surface are only about 7% of the total by SEM observation. The effect of interfacial bond strength on toughening is linked to the influence of the extent of debonding. The beneficial effect of partial debonding of the interface has been demonstrated in several model systems [13, 21], since it will result in a larger crack opening displacement upon ductile phase rupture, and therefore a longer process zone and a higher fracture toughness. However, partial debonding of the interface is very difficult to control for the particulate ductile phase because of its spherical shape. The detrimental effect of complete interfacial debonding has been shown in several composite systems, e.g. glass–Ni [7], glass–Kovar [22, 23] and B_4C–Cu [24]. The influencing factors include the interfacial bond strength, the state of stress at the ductile phase/matrix interface, the size of the particulate ductile phase and the position that a crack intercepts a ductile particle. For example, if there is a range of particle sizes, partial debonding of the comparatively large particles will probably be accompanied by complete debonding of the relatively small particles. If a crack intercepts a ductile particle away from the centre of the particle, complete debonding is also liable to occur. Obviously, these are detrimental to the toughening of the composite material. Therefore, in practice it is beneficial to create strong Al_2O_3/Ni interfaces in the composites with the microstructure of discrete nickel particles.

The excellent toughness of specimen H2 is attributed to the network distribution of the nickel phase. This makes the nickel phase more continuous and plate-like, and therefore increases the gauge length of the ductile nickel. In the case of small gauge lengths of the ductile phase, if interfacial bonding is not strong enough, the ductile phase is very liable to be pulled out, hindering its contribution to toughening. However, in the case of large gauge lengths of the ductile phase, even if interfacial bonding between the ductile phase and the brittle matrix is weak, the ductile phase is difficult to pull out. In addition, partial debonding at the interface can increase further the contribution of the ductile phase to the toughening of the composite. Bridging of cracks by the nickel phase can be observed frequently in specimen H2 (Fig. 11), indicating that it is difficult for the cracks to avoid the nickel. Fig. 12 shows the fracture surface of specimen H2. The nickel phase, mostly in the shape of plates, has been stretched to failure by necking to a line and has been extensively plastically deformed. This has been aided by partial debonding at the interface and contributes greatly to the toughness of the composite.

The toughness increment and the process zone length of the composite is determined by the ductility, the gauge length and strain state of the ductile phase, as well as the interfacial bond strength between ductile phase and brittle matrix. It is desirable to obtain maximum toughness instantly, i.e. a very short process zone is highly desirable. For the particulate dispersion microstructure (specimen H1), for a 1 mm crack length the fracture resistance is about 4 MPa $m^{1/2}$ (Fig. 7). For the network microstructure (specimen H2), the fracture resistance at 1 mm crack length is 8.3 MPa $m^{1/2}$ (Fig. 7), twice as much as that for specimen H1. Therefore, the network microstructure has a more desirable *R*-curve behaviour than the particulate dispersion microstructure.

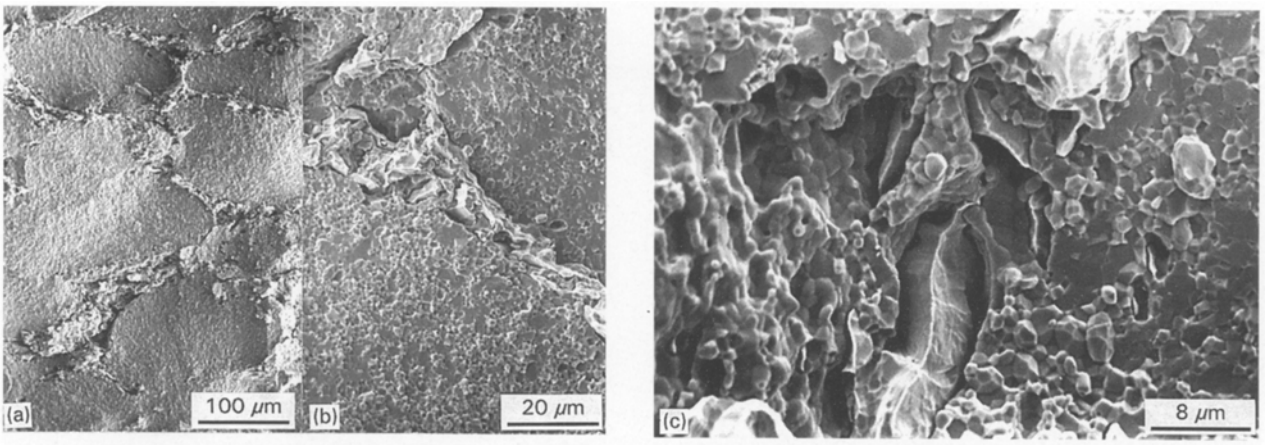

Figure 12 (a–c) Different magnifications of SEM photomicrographs showing the fracture surface of specimen H2.

4. Conclusions

Al_2O_3–Ni composite materials have been made by a hot pressing technique. Two composite microstructures, i.e. a dispersive distribution of nickel particles and a network distribution of nickel particles in an alumina matrix, have been produced. The composite specimens have densities close to the theoretical one. The hardness values of all the composite specimens are lower than the values for pure alumina. The fracture toughness of the composite materials has been measured by a double cantilever beam method. The composites have been found to be tougher than the virgin alumina matrix. The fracture toughness of the composite with a network microstructure is much higher than the composite with a microstructure of dispersed particles. For the particulate dispersion microstructure, the main limitation to toughening is the lack of plastic deformation of the ductile nickel due to the pull out of nickel particles, indicating weak bonding at the Al_2O_3/Ni interface. For the network microstructure composite, the gauge length of the ductile phase is much larger, allowing the ductile nickel to be stretched to failure between the crack faces. A large extent of plastic deformation of the nickel has been observed. The weak bonding at the Al_2O_3/Ni interface can promote partial debonding and contribute further to toughening in the network microstructure composite.

Acknowledgements

This work was supported by the Committee of Vice Chancellors and Principals (ORS award), the University of Surrey (University Scholarship), the Henry Lester Trust and Universities' China Committee. We are pleased to acknowledge the support of The Microstructural Studies Unit, University of Surrey.

References

1. M. RÜHLE and A. G. EVANS, *Prog. Mater. Sci.* **33** (1989) 85.
2. P. HING and G. W. GROVES, *J. Mater. Sci.* **7** (1972) 427.
3. M. S. NEWKIRK, A. W. URQUART and H. R. ZWICKER, *J. Mater. Res.* **1** (1986) 81.
4. B. D. FLINN, M. RÜHLE and A. G. EVANS, *Acta Metall.* **37** (1989) 3001.
5. D. C. HALVERSON, A. PYZIK, I. A. AKSAY and W. E. SNOWDEN, *J. Amer. Ceram. Soc.* **72** (1989) 775.
6. A. K. BHATTACHARYA and J. J. PETROVIC, *J. Mater. Sci.* **27** (1992) 2205.
7. V. V. KRSTIC, P. S. NICHOLSON and R. G. HOAGLAND, *J. Amer. Ceram. Soc.* **64** (1981) 499.
8. X. SUN, P. A. TRUSTY, J. A. YEOMANS and H. R. SHERCLIFF, in *Proceedings of the ICCM/VIII*, Honolulu, July 1991, edited by S. W. Tsai and G. S. Springer (SAMPE, 1991) p. 17J1–10.
9. X. SUN and J. A. YEOMANS, *Special Ceram.* **9** (1990) 297.
10. B. D. FLINN, C. S. LO, F. W. ZOK and A. G. EVANS, *J. Amer. Ceram. Soc.* **76** (1993) 369.
11. Z. CHEN and J. J. MECHOLSKY, *ibid.* **76** (1993) 1258.
12. V. D. KRSTIC, *Phil. Mag.* **A 48** (1983) 695.
13. M. F. ASHBY, F. J. BLUNT and M. BANNISTER, *Acta Metall.* **37** (1989) 1847.
14. ASM Handbook, "Metals Handbook, Properties and Selection: Non-ferrous Alloys and Pure Metals", Vol. 2, Ninth Edn (American Society for Metals, Metals Park, OH 1979) p. 777.
15. R. MORRELL "Handbook of Properties of Technical & Engineering Ceramics. Part 2: Data Reviews: Section I: High-alumina Ceramics" (HMSO, 1987) p. 59.
16. P. A. TRUSTY, PhD thesis, University of Surrey (1994).
17. M. H. LEWIS, R. H. SEEBOHM and J. W. MARTIN, *Powder Metall.* **10** (1962) 87.
18. J. A. DROMSKY, F. V. LENEL and G. S. ANSELL, *Trans. Amer. Inst. Min. Metall. Eng.* **224** (1962) 236.
19. A. U. SEYBOLT, in "Oxide Dispersion Strengthening", Metal Society Conference, Vol. 49, edited by G. S. Ansell, T. D. Cooper and F. V. Lenel (Gordon & Breach, New York, 1968) p. 469.
20. R. L. MEHAN, *Metall. Trans.* **3** (1972) 897.
21. H. E. DÈVE, A. G. EVANS, G. R. ODETTE, R. MEHRABIAN, M. L. EMILIANI and R. J. HECHT, *Acta Metall. Mater.* **38** (1990) 1491.
22. T. L. JESSEN and D. LEWIS 111, *J. Amer. Ceram. Soc.* **72** (1989) 818.
23. R. H. MOORE and S. C. KUNZ, *Ceram. Eng. Sci. Proc.* **8** (1987) 839.
24. A. J. PYZIK, I. A. AKSAY and M. SARIKAYA, in "Ceramic Microstructure '86", edited by J. A. Pask and A. G. Evans (Plenum Press, New York, 1987) p. 45.

Received 2 February
and accepted 11 May 1995